

## MP2RAGE, a self bias-field corrected sequence for improved segmentation and $T_1$ -mapping at high field

José P. Marques<sup>a,b,\*</sup>, Tobias Kober<sup>a,c</sup>, Gunnar Krueger<sup>a,c</sup>, Wietske van der Zwaag<sup>a,b</sup>, Pierre-François Van de Moortele<sup>d</sup>, Rolf Gruetter<sup>a,b,e</sup>

<sup>a</sup> Laboratory for Functional and Metabolic Imaging, Ecole Polytechnique Fédérale de Lausanne, Lausanne, Switzerland

<sup>b</sup> Department of Radiology, University of Lausanne, Lausanne, Switzerland

<sup>c</sup> Advanced Clinical Imaging Technology, Siemens Medical Solutions-CIBM, Lausanne, Switzerland

<sup>d</sup> CMRR, University of Minnesota, Minneapolis, Minnesota, USA

<sup>e</sup> Department of Radiology, University of Geneva, Geneva, Switzerland

### ARTICLE INFO

#### Article history:

Received 12 July 2009

Revised 30 September 2009

Accepted 1 October 2009

Available online 9 October 2009

### ABSTRACT

The large spatial inhomogeneity in transmit  $B_1$  field ( $B_1^+$ ) observable in human MR images at high static magnetic fields ( $B_0$ ) severely impairs image quality. To overcome this effect in brain  $T_1$ -weighted images, the MPRAGE sequence was modified to generate two different images at different inversion times, MP2RAGE. By combining the two images in a novel fashion, it was possible to create  $T_1$ -weighted images where the result image was free of proton density contrast,  $T_2^*$  contrast, reception bias field, and, to first order, transmit field inhomogeneity.

MP2RAGE sequence parameters were optimized using Bloch equations to maximize contrast-to-noise ratio per unit of time between brain tissues and minimize the effect of  $B_1^+$  variations through space. Images of high anatomical quality and excellent brain tissue differentiation suitable for applications such as segmentation and voxel-based morphometry were obtained at 3 and 7 T.

From such  $T_1$ -weighted images, acquired within 12 min, high-resolution 3D  $T_1$  maps were routinely calculated at 7 T with sub-millimeter voxel resolution (0.65–0.85 mm isotropic).  $T_1$  maps were validated in phantom experiments. In humans, the  $T_1$  values obtained at 7 T were  $1.15 \pm 0.06$  s for white matter (WM) and  $1.92 \pm 0.16$  s for grey matter (GM), in good agreement with literature values obtained at lower spatial resolution. At 3 T, where whole-brain acquisitions with 1 mm isotropic voxels were acquired in 8 min, the  $T_1$  values obtained ( $0.81 \pm 0.03$  s for WM and  $1.35 \pm 0.05$  for GM) were once again found to be in very good agreement with values in the literature.

© 2009 Elsevier Inc. All rights reserved.

### Introduction

In the past decade, the magnetization-prepared rapid gradient echo, MPRAGE (Mugler and Brookeman, 1990), sequence has become one of the most commonly used sequences to obtain  $T_1$ -weighted anatomical images of the human brain, in particular at high magnetic field. MPRAGE images are routinely used as anatomical reference for fMRI or for brain tissue classification in voxel-based morphometry (Ashburner and Friston, 2000). However, at high static magnetic fields ( $\geq 3$  T), the increased inhomogeneity of the transmit  $B_1^+$  and receive  $B_1^-$  fields creates intensity variations throughout the image (bias field). Bias fields not only render segmentation and quantitative analysis difficult but also severely affect image quality at ultra-high fields ( $\geq 7$  T). The use of adiabatic

pulses to perform the inversion in the MPRAGE is only partially able to mitigate the effects of inhomogeneous  $B_1$ .

A number of strategies have been proposed to minimize or to correct bias fields generated by the inhomogeneity of the  $B_1$  fields. Most correction strategies aim at correcting the combined (transmit and receive) bias field via post-processing techniques. This can be done either by low-pass filtering (Cohen et al., 2000; Wald et al., 1995) or by fitting slowly varying functions such as Gaussians or low order polynomials (Styner et al., 2000). The result from these low pass filters or fits is then subtracted from the original image. Such approaches can be performed iteratively together with the segmentation process (Ashburner and Friston, 2005) in which case the quality of the estimated bias field is measured by the resulting image intensity distribution. Although such approaches can improve image quality, they also tend to affect the spatial characteristics of the resulting image (Belaroussi et al., 2006). To correctly deal with  $B_1$ -induced inhomogeneities, transmit and receive inhomogeneities should be addressed separately and explicitly due to their different

\* Corresponding author. Station 6, CH-1015 Lausanne, Switzerland. Fax: +41 21 6937960.

E-mail address: [jose.marques@epfl.ch](mailto:jose.marques@epfl.ch) (J.P. Marques).

nature and implications on the signal intensity and contrast. Although transmit and receive  $B_1$  fields can be numerically calculated (Vaughan et al., 2001), such simulations require a priori knowledge of the distribution of brain tissues and their conductivity as well as complete characterization of the used RF coils. Reception  $B_1$  inhomogeneities only affect the signal amplitude of the image by a multiplicative factor related to the coil sensitivity, therefore, coil sensitivity maps could be used to correct such reception inhomogeneity (Axel et al., 1987; Roemer et al., 1990). These methods are only valid at low magnetic fields, where the ground truth of “a flat” coil sensitivity is given by the reception with a volume coil. At high fields, the lack of a ground truth makes the task of calculating an absolute coil sensitivity map more intricate. Transmission  $B_1$  inhomogeneities are more complex to correct as, for example, the  $T_1$  weighting of the sequence is closely linked to the local flip angle implying that the  $T_1$  weighting throughout the image will be different. Therefore, although many techniques exist to calculate the transmission  $B_1$  field, for example (Stollberger and Wach, 1996), to correct its implication on the image intensity, it is also necessary to have prior knowledge of the contrast dependence on the flip angle (Wang et al., 2005). A recent promising technique is to, instead of correcting a posteriori, effectively reduce the inhomogeneity by performing parallel transmission (Katscher and Bornert, 2006). Due to the complexity and expensiveness of the hardware necessary to perform parallel transmission, the technique is not yet widely available. Another approach to deal with the transmission inhomogeneity is to carefully adjust the amplitude of the various RF pulses used in the sequence so that the resulting contrast is less dependent on the local flip angle accuracy (Thomas et al., 2005; Van de Moortele et al., 2009), which is the approach that will be pursued in this manuscript.

Recently, an extension of the MPRAGE sequence, which performs the acquisition of 2 volumes after each inversion (see Fig. 1), has been proposed (Marques et al., 2008; Van de Moortele et al., 2008, 2009). In this article, this sequence will be referred as MP2RAGE (Magnetization Prepared 2 Rapid Acquisition Gradient Echoes).

In a conventional MPRAGE, the signal is not exclusively dependent on  $T_1$  contrast but also on  $M_0$  (often referred to as proton density) and  $T_2^*$ . Both  $M_0$  and  $T_2^*$  tend to reduce the available  $T_1$  contrast of the MPRAGE image as the values of  $M_0$  and  $T_2^*$  of cerebral spinal fluid (CSF), grey matter (GM), and white matter (WM) decrease in this order. On the other hand, if two MPRAGE images are acquired at two different inversion times, but have otherwise the identical sequence parameters, they will be affected in identical

manner by  $B_1^-$ ,  $M_0$  and  $T_2^*$  and thus, a combined image by means of a ratio will be independent of  $B_1^-$  as well as  $M_0$  and  $T_2^*$  (Van de Moortele et al., 2009).

One way of acquiring bias field-independent images is to perform quantitative imaging, of which  $T_1$  mapping is a popular example due to its high tissue contrast. Various  $T_1$  mapping techniques have been developed throughout the years. Typically  $T_1$  is estimated using variations of either inversion recovery or saturation recovery sequences or based on variable flip angle spoiled gradient echoes (Christensen et al., 1974). The most common variations of the inversion recovery technique are the Look-Locker approaches (Look and Locker, 1970), where multiple RF pulses are applied during the recovery process allowing for a faster measurement of the longitudinal recovery process. This concept has been combined with EPI (Gowland and Mansfield, 1993) or with flash readout (Deichmann et al., 1999). While EPI-based methods offer the quickest method for  $T_1$  mapping, they suffer from severe distortions, and the  $T_1$  maps in regions with tissue partial volumes will bias the  $T_1$  to the tissue with the longest  $T_2^*$  due to the inherently long echo times of the EPI readout. Recently, spoiled gradient echo methodologies to perform  $T_1$  mapping have also successfully been brought into clinical practice (Deoni, 2007; Deoni et al., 2005), allowing high-resolution whole-brain  $T_1$  maps to be acquired in  $\sim 10$  min. One of the drawbacks of this technique is that, as it requires various sequences to be applied, the need to co-register the images due to inter-scan motion implies an effective decrease of the spatial resolution.

Since the MP2RAGE resulting image is to a large extent purely  $T_1$  weighted, it provides excellent base for fast  $T_1$  estimation. The goal of this study was to optimize the parameters that render a bias free  $T_1$ -weighted whole-brain image that allows calculation of  $T_1$  relaxation time at high spatial resolution ( $<1$  mm<sup>3</sup>) in  $\sim 10$  min in one sequence, without the need to co-register images, facilitating online  $T_1$  calculations. The proposed method was validated in phantoms by comparison to standard  $T_1$  maps (inversion recovery EPI based) and in vivo by comparison to brain tissue  $T_1$  values found in literature for both at 3 and 7 T.

## Methods

The MP2RAGE sequence shown in Fig. 1, as the conventional MPRAGE, starts with a magnetization preparation performed with an adiabatic inversion and, after a delay TA, a gradient echo block is introduced. This low flip angle gradient echo block has a short repetition time, TR, and is repeated nPE2 times stepping linearly

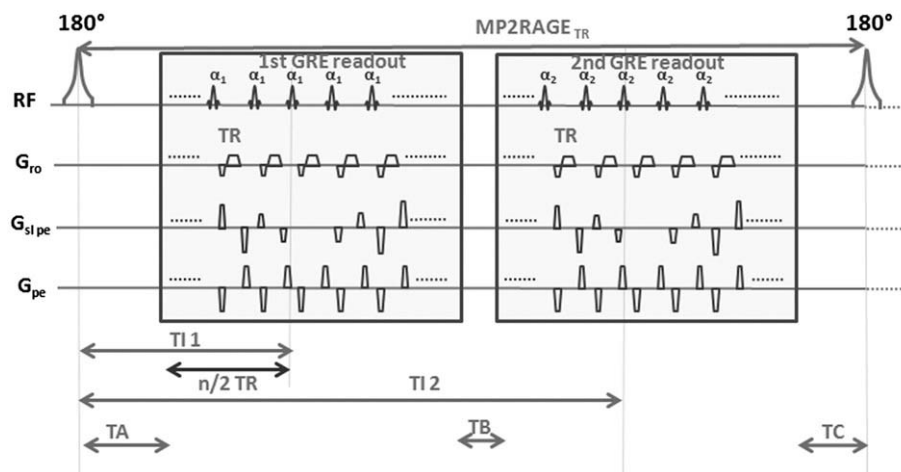


**Fig. 1.** Diagram of the MP2RAGE sequence. Inversion times  $T_{I1}$  and  $T_{I2}$  are defined as the time from the middle of the inversion pulse to the excitation corresponding to the center k-space line in the phase encoding in the slab selection direction. MP2RAGE<sub>TR</sub> is the time between two successive inversion pulses and TR is the time between successive excitation pulses in the GRE kernel, which is composed of n excitations.

through the whole second-phase encoding direction. The center of k-space in this direction defines the effective inversion time  $T_{I1}$ . At the end of the first rapid gradient echo block, a delay is introduced,  $T_B$ , before the start of the second gradient-echo block that is identical to the first gradient-echo block except for its flip angle. At the end of the second gradient-echo block, a recovery time,  $T_C$ , is introduced before the adiabatic inversion is reapplied. This process is repeated  $nPE3$  times in order to sample the k-space in the third dimension (for a mathematical description of the expected signal, see Appendix 1).

The two images acquired at  $T_{I1}$  and  $T_{I2}$  are subsequently combined using the following expression:

$$MP2RAGE = \frac{GRE_{T_{I1}} GRE_{T_{I2}}}{GRE_{T_{I1}}^2 + GRE_{T_{I2}}^2} \quad (1)$$

Eq. (1) has the convenient property of limiting the possible values of the MP2RAGE between  $-0.5$  and  $0.5$  (even in regions dominated by noise) resulting in a predefined range of image intensities. For example, when compared to a simple ratio expression, that diverges whenever the second image approaches zero, Eq. (1) has only one point of singularity ( $GRE_{T_{I1}} = GRE_{T_{I2}} = 0$ ) and even as it approaches this singularity, the values are still within the range  $-0.5$  to  $0.5$ , facilitating the choice of dynamic range in which to display the image. For image intensities where  $abs(GRE_{T_{I2}}) > 4 abs(GRE_{T_{I1}})$ , the result will be close to the simple ratio (within 10%) and the SNR of the combination image will be essentially equivalent. For image intensities where  $abs(GRE_{T_{I2}})$  is equal to 4, 2, 1.5, and 1.25 times the  $abs(GRE_{T_{I1}})$ , the SNR of the combined MP2RAGE image will be superior to that of a simple ratio by a factor  $\sim 1.25$ ,  $\sim 1.75$ ,  $\sim 2.5$ , and  $\sim 5$  respectively (for more details see Appendix 2).

Although image combination may result in a reduction of SNR in the final image due to noise propagation, because the dependence in  $M_0$  and  $T_2^*$  (that reduces contrast in MPRAGE type sequences) was removed from the combined MP2RAGE image, it does not necessarily imply reduction of contrast-to-noise ratio of the combined image. To further improve the contrast-to-noise ratio between white matter, grey matter and CSF, their MP2RAGE (Fig. 1) signal amplitudes were numerically calculated by solving the Bloch equations (see Appendix 1). The signal was considered to come from the center k-space point (Deichmann et al., 2000). The effects of different echo times (TE) and apparent relaxation times ( $T_2^*$ ) and reception sensitivity ( $B_1^-$ ) were ignored as their effect will be cancelled after the image combination (Eq. 1, see Appendix 1 for further details). To find the optimum parameters for the MP2RAGE sequence, the goal was to maximize contrast-to-noise ratio per unit of time between different tissues in the final image. Contrast-to-noise ratio per unit of time between two tissues in the final image was defined as:

$$CNR_{tissue1VsTissue2} = \frac{MP2RAGE_{tissue1} - MP2RAGE_{tissue2}}{\sqrt{\sigma_{tissue1}^2 + \sigma_{tissue2}^2}} \cdot \frac{1}{\sqrt{MP2RAGE_{TR}}} \quad (2)$$

Where  $\sigma$  stands for the noise of the MP2RAGE signal and was estimated via error propagation of Eq. (1). As the aim of this article is the application of the MP2RAGE sequence for 3D high-resolution brain imaging at high fields, some parameters were fixed:

- (i) Number of excitations per GRE module,  $n$ , was set to 160 or 256 and the TR of the GRE module was set to 7 ms;
- (ii)  $T_1$  values were assumed to be of WM/GM/CSF = 1.05/1.85/3.35 s at 7 T and 0.85/1.35/2.5 at 3 T;
- (iii) The inversion efficiency of the adiabatic pulse was assumed to be total.

The following parameters were varied:

- (i) The repetition time MP2RAGE TR (Fig. 1) was varied from 4 to 12 s in steps of 0.25 s;

- (ii)  $T_{I1}$  and  $T_{I2}$  were varied from  $nTR/2$  to MP2RAGE TR-  $nTR/2$  in steps of 100 ms while keeping the condition  $T_{I2} - T_{I1} > nTR$  true;
- (iii)  $\alpha_1$  and  $\alpha_2$  were independently varied from 1–15 degrees.

The parameters MP2RAGETR,  $T_{I1}$ ,  $T_{I2}$ , for all possible combinations of  $\alpha_1$  and  $\alpha_2$  were chosen from simulations in order to optimize the CNR per unit time between GM-WM and CSF-GM.

To estimate the range of  $B_1^+$  inhomogeneity and accuracy of the automatic setting of the reference voltage,  $B_1^+$  maps were calculated using a double-angle method technique (Stollberger and Wach, 1996). Two EPI volumes of 36 slices of slice thickness 2 mm and  $2 \times 2$  mm in plane resolution (matrix  $96 \times 96$ ) were acquired with TR/TE = 30s/19 ms and flip angles 60 and 120 degrees, respectively. Local  $B_1^+$  fraction was defined for our specific case (first flip angle =  $\pi/3$ ) as  $\frac{3}{\pi} \arccos\left(\frac{image_{120}}{2 image_{60}}\right)$ . Subsequently, the distributions of the local  $B_1^+$  fraction values inside the brain (threshold masked after visual inspection of each image) were characterized by their mean and standard deviation. To reduce the variability in MP2RAGE signal intensity, due to  $B_1$  inhomogeneity, a grid search over flip angles was performed. The aim was to reduce the signal variation of any of the tissues (due to a range of  $B_1$  from 0.8 to 1.2 at 3 T and 0.6 to 1.4 at 7 T) below 5% (for 3 T) and 7% (for 7 T) without significantly decreasing the CNR (accepted reduction of 15%).

MP2RAGE was implemented on a 3 T (Trio a Tim System) and 7 T (7T Tim System) MR scanners (Siemens Medical Solutions, Erlangen, Germany) operating with the Syngo VB15 software.

At 3 T, data from five healthy male subjects ( $34 \pm 5$  years) were acquired using a 32-channel head coil. At 7 T, seven subjects (6 males and one female,  $25 \pm 4$  years) were acquired using a transmit-receive 8-channel head coil (RAPID MR International, Germany). All subjects provided written informed consent prior to the imaging session. The study was approved by the institutional review board of the CHUV. The different sequence parameters used at the different fields for the different subjects are described in detail in Table 1.

The complex images were combined to calculate the MP2RAGE image as follows:

$$S = \text{real}\left(\frac{GRE_{T_{I1}}^* GRE_{T_{I2}}}{|GRE_{T_{I1}}|^2 + |GRE_{T_{I2}}|^2}\right) \quad (3)$$

Where  $GRE_{T_{I1}}^*$  stands for the complex conjugate of  $GRE_{T_{I1}}$ . Eq. (3) has the advantage of removing phase terms due to  $B_0$  inhomogeneities, while keeping the information of whether there was a phase change between the first to second inversion times.

To calculate  $T_1$  maps, the sequence parameters given in Table 1 were taken into account as well as the inversion efficiency of the truncated hyperbolic secant adiabatic inversion pulse, which was established by numerical simulations at 0.96. Bloch simulations were performed for the MP2RAGE sequence using the equations described in detail in the Appendix, and the  $T_1$  value of each pixel was estimated via linear interpolation. Bloch simulations and  $T_1$  estimation were integrated in the online image reconstruction on the scanner providing the calculated  $T_1$  maps directly at the end of the scan.

To estimate the range of precision of the MP2RAGE  $T_1$  values and evaluate its performance in the presence of noise, numerical simulations were performed for the MP2RAGE parameters proposed for 3 and 7 T, respectively. The Bloch simulations were performed for different values of  $T_1$  ranging from 0.1 to 5 s. Independent Gaussian distributed noise was added to the first and second inversion time signals. The noise level added to each contrast was the same. The SNR of the simulation was defined as the ratio of the signal of the second inversion time divided by the noise standard deviation (which implies that the SNR of the first image is smaller than the reported value). Subsequently, the MP2RAGE signal was computed as in Eq. (1), and a  $T_1$  value was estimated as described above. For each  $T_1$  value and

**Table 1**  
MP2RAGE acquisition parameters as used for the data presented in Figs. 7 and 8 and Table 2.

Field	Subject	Parameters	MP2RAGE <sub>TR</sub> (s)	T <sub>1</sub> (s)	T <sub>2</sub> (s)	$\alpha_1$ (deg)	$\alpha_2$ (deg)	TR (ms)	N <sub>slices</sub>	Resolution (mm <sup>3</sup> )	Fat suppression	iPAT	Partial Fourier
3 T	1-4 P		6.75	0.8	3.2	4	4	7.9	160	1	yes	3	6/8
3 T	5	1	6.25	0.8	2.2	7	5	5.8	160	1	no	3	6/8
3 T	5	2	6.25	0.8	2.2	4	5	5.8	160	1	no	3	6/8
3 T	5	3	5	0.7	2.0	4	5	5.8	160	1	no	3	8/8
3 T	5	4	4	0.6	1.8	4	5	5.8	160	1	no	2	7/8
7 T	1-7 P		8.5	1	3.5	4	4	7.2	176	0.5–0.8	yes	3	6/8
7 T	8	1	8.25	1	3.3	7	5	6.9	160	1	yes	3	6/8
7 T	8	2	8.25	1	3.3	4	5	6.9	160	1	yes	3	6/8

noise level, this process was repeated 100 times. The mean and standard deviation of the MP2RAGE T<sub>1</sub> over the 100 simulations were computed.

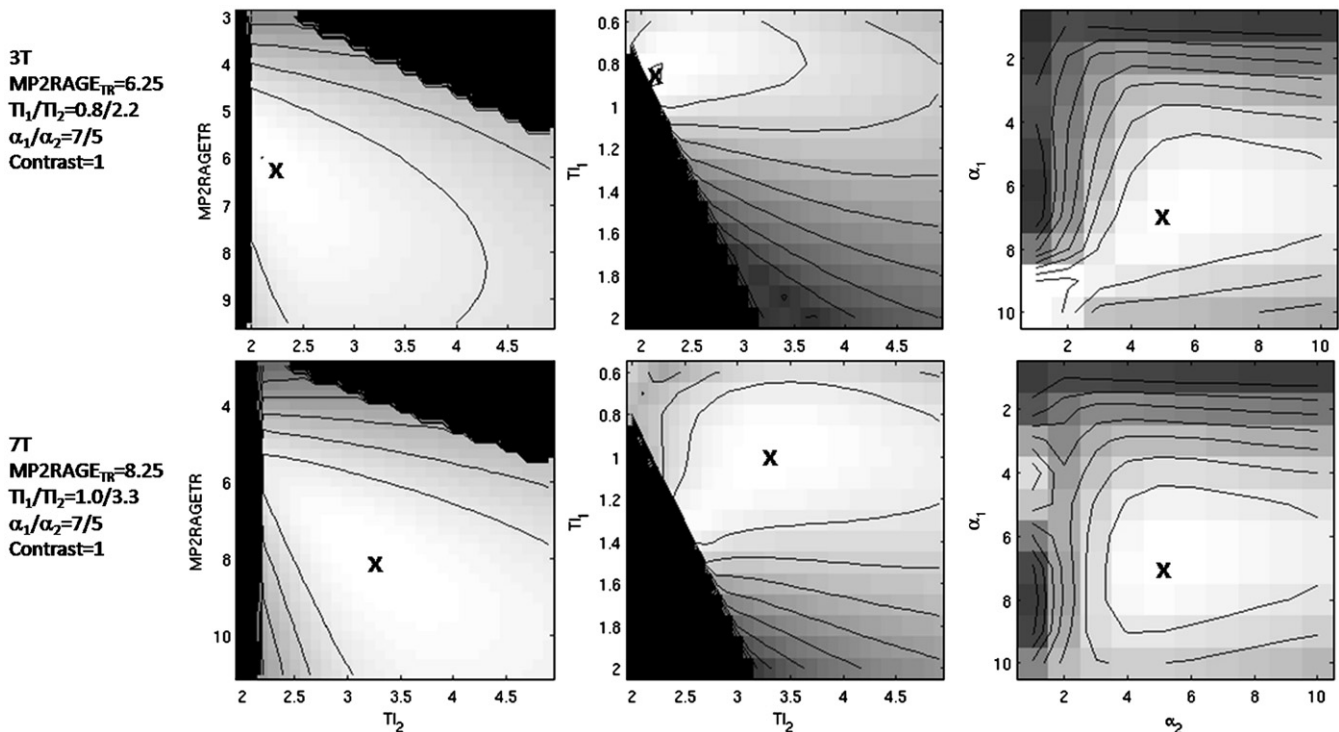
To validate the MP2RAGE T<sub>1</sub> measurements, a head phantom was scanned at 3 and 7 T using the MP2RAGE sequence and a single-slice inversion recovery spin echo EPI (IR-EPI) with varying inversion times. The head phantom contained four different compartments with Agar (2.2%, 3.6%, 4.6%, 3.4%) doped with gadolinium (0, 6, 9, 14  $\mu$ l/50ml). B<sub>1</sub> maps as described above were used to select an imaging slice with similar B<sub>1</sub> distributions to those found in the human head. Other acquisition parameters for the IR-EPI: TR = 30s; slice thickness 3 mm; FOV = 300 × 300 mm; matrix size = 96 × 96; TI = 0.02/0.12/0.32/0.52/0.82/1.22/1.62/2.02/2.52/3.00/3.50/4.00/5.00 s. MP2RAGE parameters are given in Table 1 (subject P). The corresponding slice of the MP2RAGE T<sub>1</sub> map was co-registered to the IR-EPI T<sub>1</sub> map. Regions containing no signal and edges of the compartments were masked out to reduce the effect of registration problems due to the increased distortions in the IR-EPI T<sub>1</sub> map. Finally, T<sub>1</sub> values in two computed T<sub>1</sub> maps were compared on a pixel-by-pixel basis and the correlation between the two T<sub>1</sub>-value distributions was calculated.

Image intensity histograms of the brain were created to further evaluate the quality of the bias field cancellation, the contrast quality

for segmentation purposes and the reliable T<sub>1</sub> quantification. GRE<sub>T12</sub> images were skull stripped using BET (Smith, 2002), the brain mask obtained was applied to the MP2RAGE images and T<sub>1</sub> maps so that only brain tissues were considered in the histograms. To compare the T<sub>1</sub> values obtained to those found in literature, regions of interest were drawn in the MP2RAGE images using fslview ([www.fmrib.ox.ac.uk](http://www.fmrib.ox.ac.uk)) covering the following regions: frontal white matter, corpus callosum, nucleus caudate, putamen, pallidum, thalamus, temporal cortex grey matter, and motor cortex grey matter. Average T<sub>1</sub> values were obtained for all ROIs.

## Results

The optimization of the contrast-to-noise ratio (CNR) of the MP2RAGE image was performed as a function of five variables, rendering its visualization rather complex. In Fig. 2, it is possible to see representations of the dependence of the CNR as a function of two variables at a time, keeping the remaining three variables fixed at the values described on the left column. One conclusion that can be drawn from Fig. 2 is that CNR is a smooth and slow varying function of the inversion times, flip angles, and MP2RAGE<sub>TR</sub>, as is clear from the large regions above 90% of the maximum CNR. This implies some flexibility to, for example, choose a shorter MP2RAGE<sub>TR</sub>. The optimum contrast-



**Fig. 2.** Maps of the contrast-to-noise ratio (CNR) per unit of time as a function of MP2RAGE<sub>TR</sub> and T<sub>2</sub> (first column), T<sub>1</sub> and T<sub>2</sub> (second column),  $\alpha_1$  and  $\alpha_2$  (third column). First and second rows show CNR maps for 3T and 7T relaxation parameters, respectively. The contour lines are set at 10% intervals to the maximum available contrast at the respective field. Maximum available contrast is shown with crosses.

to-noise ratio between CSF, GM, and WM, considering the assumptions described in the methods section, was found to be obtained with the following parameters:

- a) at 3 T,  $MP2RAGE_{TR} = 6.25$  s  $TI_1/TI_2 = 0.8/2.2$  s,  $\alpha_1/\alpha_2 = 7^\circ/5^\circ$ ;
- b) at 7 T,  $MP2RAGE_{TR} = 8.25$  s  $TI_1/TI_2 = 1.0/3.3$  s,  $\alpha_1/\alpha_2 = 7^\circ/5^\circ$ ;

Because the long  $MP2RAGE_{TR}$  can make the total acquisition time rather long, a protocol with a maximum  $MP2RAGE_{TR}$  of 5 s was derived. The optimum protocols under this constraint were as follows: at 3 T,  $MP2RAGE_{TR} = 5$  s  $TI_1/TI_2 = 0.7/1.5$  s,  $\alpha_1/\alpha_2 = 7^\circ/5^\circ$ ; at 7 T,  $MP2RAGE_{TR} = 5$  s  $TI_1/TI_2 = 0.7/2.5$  s,  $\alpha_1/\alpha_2 = 7^\circ/5^\circ$ . This reduction in  $MP2RAGE_{TR}$  has a cost of 3% and 7%, respectively, on CNR but allows a significant reduction of the total acquisition time or reduction of the acceleration factors needed.

At 3 T, the shorter  $T_1$ s allowed to further reduce the repetition time to 4 s. For the same total acquisition time, the CNR was reduced by 9% in respect to the optimum 3 T acquisition parameters. Note that the CNR per unit of time used in the above optimizations means that these values assume equivalent total acquisition times. For example, at 7 T, assuming 256 phase encode steps are needed, no partial k-space sampling is performed and that the aim is to perform the study in 7 min, protocols with  $MP2RAGE_{TR}$  8.25 or 5 s would require acceleration factors,  $R$ , of 5 or 3, respectively. The CNR per unit of time calculated

above is independent of the acceleration factor  $R$  but will be affected by the  $g$  factor,  $g_R$ , as  $CNR_{MP2RAGE_{TR}}/g_R$ . For most coil arrangements, the deterioration associated with such high acceleration factors due to  $g_R$  will outweigh the gain in CNR associated with the longer  $MP2RAGE_{TR}$ , effectively favoring a shorter TR protocol.

As mentioned in the Methods section, the bias field introduced by the reception field is just a multiplicative factor and will be completely removed by eq. (1). On the other hand, the transmit field inhomogeneities will effectively change the contrast and will have different effects on the first and second contrasts. Based on  $B_1^+$  maps acquired, the  $B_1$  fraction was found to have a standard deviation of  $0.10 \pm 0.01$  and  $0.23 \pm 0.1$  at 3 and 7 T, respectively. This analysis allowed us to conclude that at 3 and 7 T, the distribution >95% of the brain voxels are within the  $\pm 20\%$  and  $\pm 40\%$   $B_1^+$  variation at 3 and 7 T. The grey boxes in Fig. 3 show the expected spread of signal intensities for the different tissues in the  $MP2RAGE$  image due to transmission inhomogeneity at 3 T (Fig. 3a) and 7 T (Fig. 3b). The lightest, outer, grey lines correspond to a  $B_1$  inaccuracy of  $\pm 20\%$  and  $\pm 40\%$  for 3 and 7 T. Such a spread of image intensities is detrimental for automated tissue classification as an unambiguous relationship between  $T_1$  and signal intensity is desired. In the  $MP2RAGE$  sequence, this can be partly compensated by varying the intensities of the flip angles used to obtain the  $GRE_{TI1}$  and  $GRE_{TI2}$  images. It was noticed that the first flip angle,  $\alpha_1$ ,

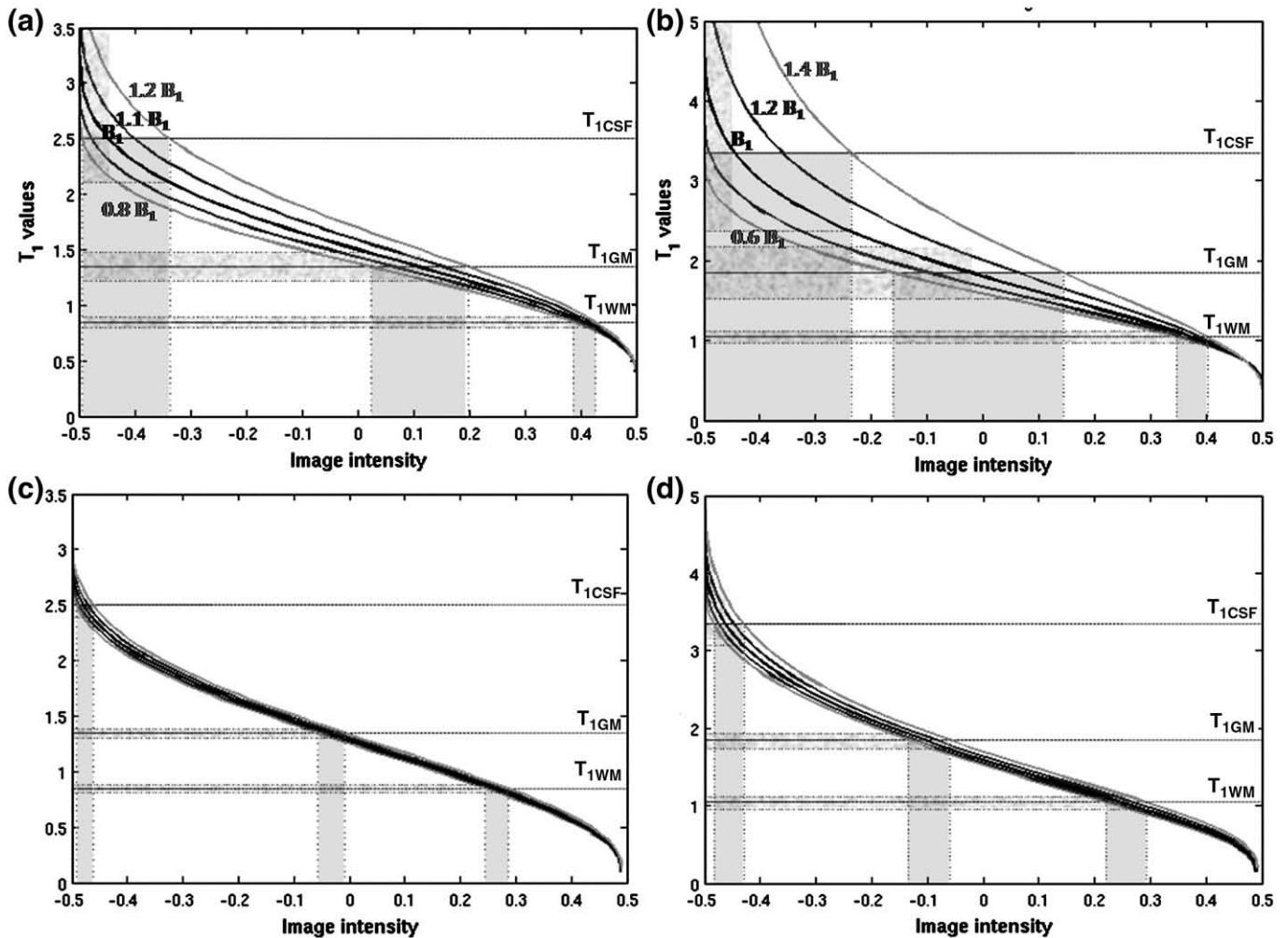


**Fig. 3.** The effect of  $B_1^+$  deviations on signal intensities and  $T_1$  estimations. The plots show signal intensity versus  $T_1$  values considering different  $MP2RAGE$  parameters: (a)  $MP2RAGE_{TR} = 6.75$  s,  $TI_1/TI_2 = 0.8/3.2$  s,  $\alpha_1/\alpha_2 = 7^\circ/5^\circ$ ; (c)  $MP2RAGE_{TR} = 6.75$  s,  $TI_1/TI_2 = 0.8/3.2$  s,  $\alpha_1/\alpha_2 = 4^\circ/5^\circ$ ; (b)  $MP2RAGE_{TR} = 8.0$  s,  $TI_1/TI_2 = 1.0/3.3$  s,  $\alpha_1/\alpha_2 = 7^\circ/5^\circ$ ; (d)  $MP2RAGE_{TR} = 8.0$  s,  $TI_1/TI_2 = 1.0/3.3$  s,  $\alpha_1/\alpha_2 = 4^\circ/5^\circ$ . Plots a, c and b, d correspond to 3T and 7T parameters, respectively. The assumed CSF, GM, and WM  $T_1$  values at those fields are shown as horizontal lines. Dark grey and light grey lines in the plots show the expected signal as a function of  $T_1$  for an effective transmission field deviation of (a, c)  $\pm 10\%$ ,  $\pm 20\%$  and (b, d)  $\pm 20\%$ ,  $\pm 40\%$ . Light grey boxes show the predicted spread of signal intensities (vertical boxes) and  $T_1$  estimations (horizontal boxes) of the different tissues due to  $B_1$  variations of (a, c)  $\pm 20\%$  and (b, d)  $\pm 40\%$ .

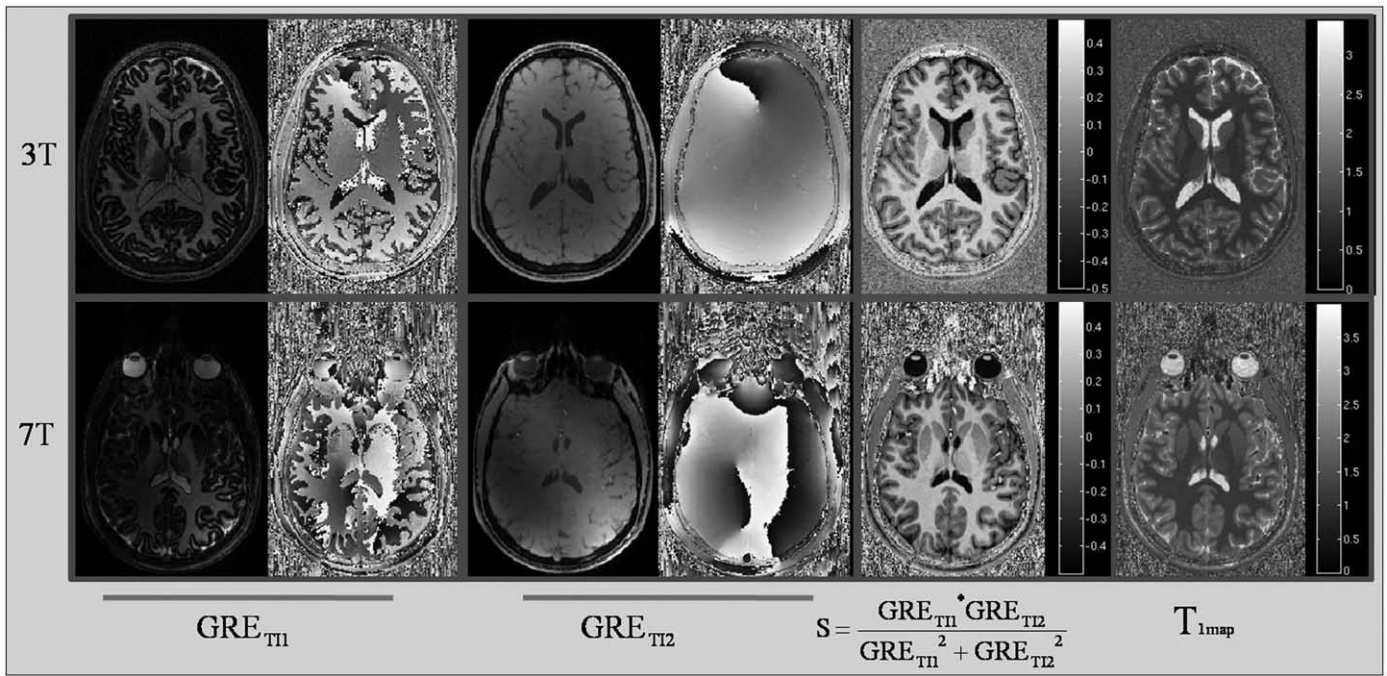


Fig. 4. Representative transverse slices obtained with the MP2RAGE sequence at 3 and 7 T, the result after combination and the T<sub>1</sub> estimation. All images are displayed using their entire dynamic range. Complex data are shown as both magnitude and phase.

had a large impact on the spread of image intensities of CSF and GM. As the first flip angle was reduced (Figs. 3c and d), the spread of image intensities was constricted.

The optimum parameters when assuming a transmission field inhomogeneity at 7 T of ± 40%, accepting a reduction of the contrast-to-noise ratio between tissues of 15%, and keeping the other sequence parameters constant, was found to be at α<sub>1</sub>/α<sub>2</sub> = 4/5. The same flip angle combination was found to successfully compensate the 3T B<sub>1</sub> field inhomogeneities (while implying 12% reduction on the contrast sensitivity). The improved insensitivity of S to B<sub>1</sub><sup>+</sup> is clear when comparing the plots on the top (MP2RAGE signal dependence for

sequence with parameters not optimized for B<sub>1</sub><sup>+</sup> inhomogeneity) and bottom (MP2RAGE signal dependence for sequence with parameters optimized for B<sub>1</sub><sup>+</sup> inhomogeneity) of Fig. 3. In the bottom plots of Fig. 3, it is possible to notice that most of the B<sub>1</sub><sup>+</sup> dependence of the MP2RAGE has been removed. At 7 T, for the B<sub>1</sub> inhomogeneity optimized parameters, the T<sub>1</sub> estimation of WM, GM, and CSF will have a variation of 3.8%, 2.5%, and 4.2% per 20% of B<sub>1</sub> variation, while at 3 T, it will have a variation of 2.2%, 1.5%, and 2.4% per 10% of B<sub>1</sub> variation.

Fig. 4 shows examples of the magnitude and phase images at the two different inversion times and after their combination through Eq.

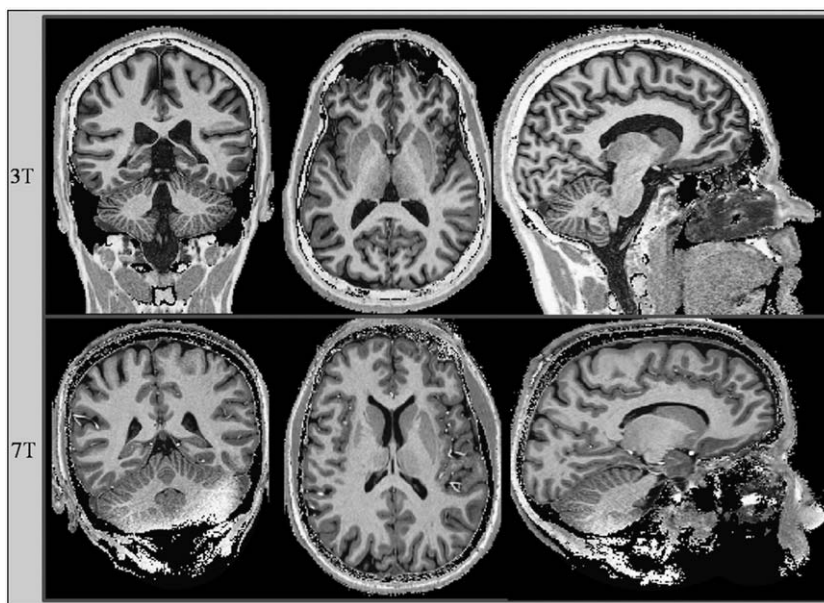
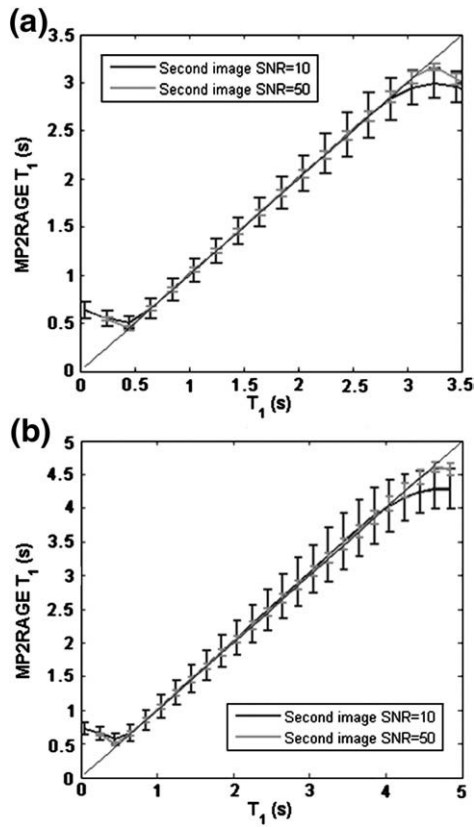


Fig. 5. Transverse, coronal, and sagittal slices taken from images acquired at 3 T (top) and 7 T (bottom). Three-Tesla data were acquired with MP2RAGE<sub>TR</sub>/T<sub>1</sub>/T<sub>2</sub> = 6.25 s/0.8 s/2.2 s, α<sub>1</sub>/α<sub>2</sub> = 4°/5°, 1 mm<sup>3</sup> without fat suppression. Seven-Tesla data were acquired with MP2RAGE<sub>TR</sub>/T<sub>1</sub>/T<sub>2</sub> = 8.0 s/1.0 s/4.0 s, α<sub>1</sub>/α<sub>2</sub> = 4°/5°, 0.73 mm<sup>3</sup> with fat suppression. Background was suppressed using a mask based on the thresholding of the second contrast image.



**Fig. 6.** Plots of the MP2RAGE T<sub>1</sub> value estimated and their standard deviations using the optimized MP2RAGE parameters derived for 3 T (a) and 7 T (b) as a function of the real T<sub>1</sub>. Black and light grey lines represent scenarios where the SNR of the second image is 10 and 50, respectively.

(3). The phase images in Fig. 4 often show phase singularity artifacts resulting from erroneous phase combination of the different coils (e.g., see arrow pointing to frontal brain area in 3-T phase map of the second contrast). To avoid image artifacts in the MP2RAGE image arising from phase singularities in the combined phase images, the images of each different coil were first combined through Eq. (3) and then the MP2RAGE images from different coils were combined, using the GRE<sub>T12</sub> as a weighting function. It is clear that the image combination (Fig. 4, second image from the right) resulted in images with both very good contrast and bias field cancellation both at 3 and 7 T. Using the lookup table created for each specific protocol (using the equation in Appendix 1), T<sub>1</sub> maps were computed. Fig. 5 shows

representative sections of 3D MP2RAGE images acquired at 3 and 7 T. Note the homogeneity of the white matter throughout the brain. In the sagittal slice of the 7-T data, artifacts can be found in the cerebellar region. This artifact results from not meeting the adiabaticity condition in this region outside the sensitive area of the transmit RF coil.

The results of the simulation of the precision and accuracy of the T<sub>1</sub> values measured in the presence of noise are displayed in Figs. 6a and b for 3 and 7 T. If the accuracy of the method is defined as (MP2RAGE T<sub>1</sub> - T<sub>1</sub>)/T<sub>1</sub>, at the low SNR level of 10, the range in which the accuracy of the method is within 2% is 0.6–3.0 s at 3 T and 0.7–4.2 s at 7 T. In this range, for an SNR level of 50, accuracy is within 0.5%. These easily cover the T<sub>1</sub> ranges for which the sequences were optimized (0.85–2.50 s at 3 T and 1.1–3.35 at 7 T). As an example, the precision, which was measured as the standard deviation over the 100 simulated measurements was found to be 0.03 s at 3 T and 0.04 s at 7 T.

To demonstrate the conformity of the MP2RAGE T<sub>1</sub> maps to standard T<sub>1</sub> maps, Fig. 7a shows a pixel-by-pixel plot of the T<sub>1</sub> values obtained with IR-EPI and MP2RAGE sequences at 3 and 7 T. The T<sub>1MP2RAGE</sub> = T<sub>1IREPI</sub> line is shown in dashed grey. The high degree of correlation between the two methods (0.99) was confirmed by linear fits (R<sup>2</sup> > 0.9) for both 3 and 7 T data. The spread in T<sub>1</sub> values within the compartments was observed in all T<sub>1</sub> maps (MP2RAGE and IR-EPI at both 3 and 7 T), and is therefore likely to be caused by settling of the Agar gel. The slices in which measured T<sub>1</sub> values were compared had a standard deviation in B<sub>1</sub> of 0.11 and 0.18 at 3 and 7 T, respectively, values that are similar to the whole head B<sub>1</sub> distributions found human subjects. This observation further demonstrates the robustness of the T<sub>1</sub> values measured despite the presence of significant B<sub>1</sub> inhomogeneities. Fig. 7b shows histograms of T<sub>1</sub> values obtained for four different subjects at 3 T using identical sequence parameters (see Table 1, subjects 1–4, at 3 T) while Fig. 7c shows data of seven subjects scanned at 7 T (see Table 1, subjects 1–7, at 7 T). At both field strengths, the T<sub>1</sub> histograms show good inter-subject reproducibility of both peak location and amplitude of the WM, GM, and CSF compartments.

Figs. 8a and c shows histograms of image intensity and T<sub>1</sub> values obtained for a single subject (subject 5, Table 1) at 3 T using different sets of sequence parameters. Any of the parameter choices gives a very good contrast between brain tissues (distinct tissue peaks), although it is clear that parameter set 1 (α<sub>1</sub>/α<sub>2</sub> = 7/5) produced a broader grey matter peak, as expected from Fig. 3a. The same behavior was found at 7 T as can be seen in Figs. 8b and d where the optimization of the RF pulse choice, significantly improved the grey–white matter peak separation. From the clear separation of grey matter, white matter, and CSF peaks, it can be concluded that the

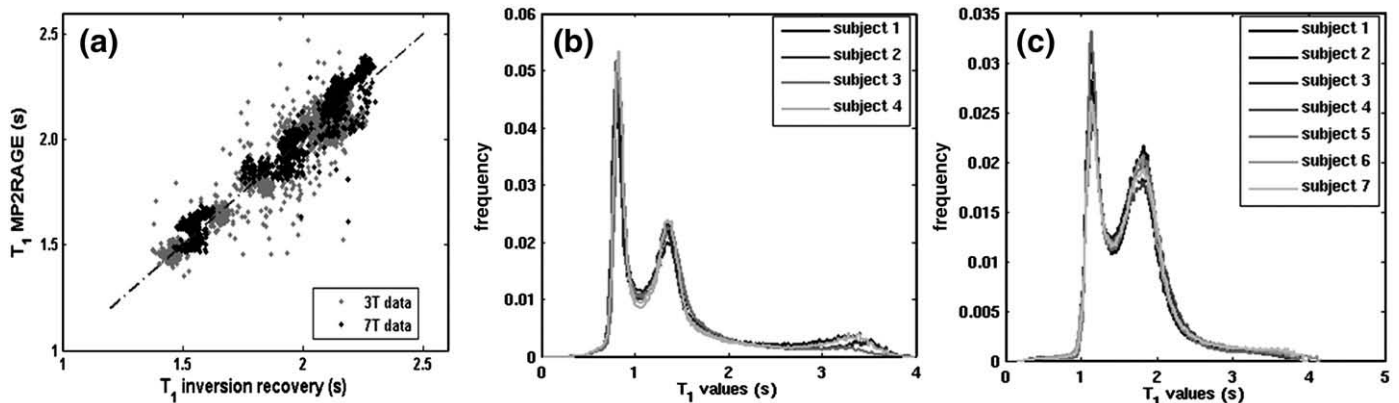


**Fig. 7.** (a) Pixel by pixel correlation of the T<sub>1</sub> maps obtained in a head phantom using the MP2RAGE and the IR-EPI at 3 T (grey dots) and 7 T (black dots). T<sub>1</sub> histograms of the entire brain after brain extraction at 3 T (b) and 7 T (c). Note the inter-subject reproducibility of the signal intensities and T<sub>1</sub> values using the sequence parameters detailed in Table 1.

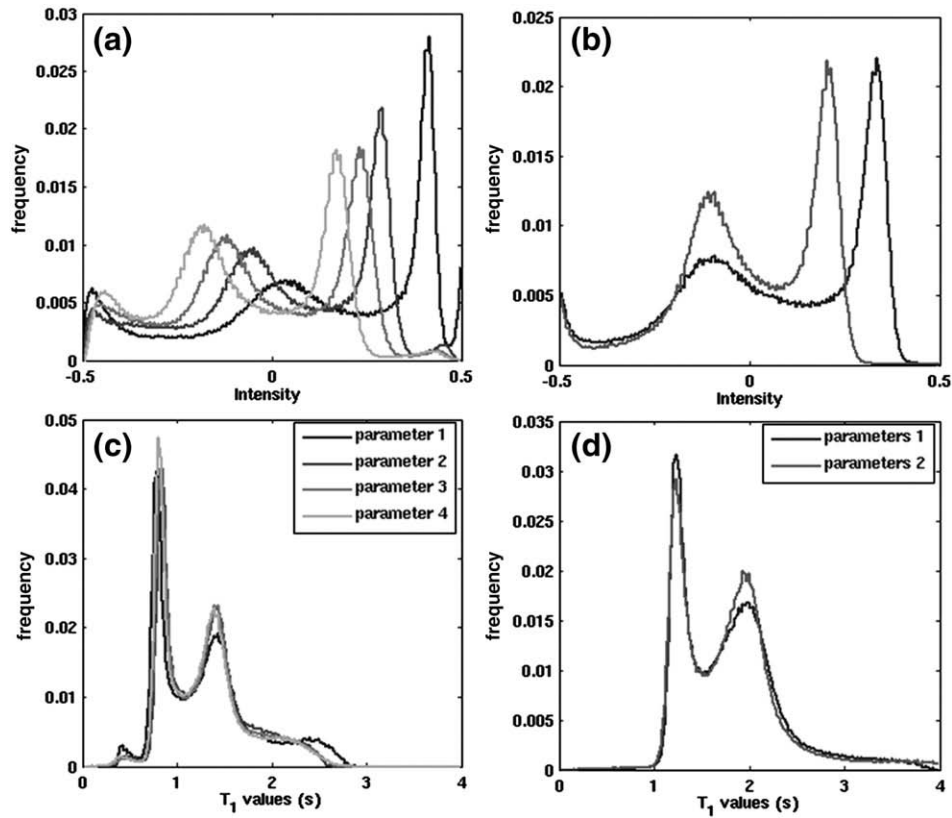


**Fig. 8.** MP2RAGE intensity (a, b) and  $T_1$  (c, d) histograms of the entire brain after brain extraction at 3 T (a, c) and 7 T (b, d). Per field, all data were acquired from a single subject. Different lines correspond to different MP2RAGE sequence parameters used as detailed in Table 1.

methodology presented here provides a good bias field cancellation and that the MP2RAGE contrast obtained can prove useful in applications such as segmentation. Note that the resulting  $T_1$  estimations were independent of the sequence parameters (position of the tissue peaks in Fig. 8c), despite the different tissue signal intensities (position of the tissue peaks in Fig. 8a) obtained with different parameter sets. Since in these acquisitions no fat suppression was used, a fourth peak was found in the histogram, corresponding to the short  $T_1$  component ascribed to fat.

Regions of interest were drawn on the  $T_1$  images to obtain  $T_1$  for different tissues at 3 and 7 T (Table 2). For comparison, Table 3 shows literature  $T_1$  values for white and grey matter, the putamen and nucleus caudate at 3 and 7 T.

To demonstrate the higher resolutions achievable with MP2RAGE at 7 T, a 0.65 mm isotropic resolution whole head scan was acquired in 12 min. Figs. 9a and b shows transverse slices of the MP2RAGE image and of the computed  $T_1$  map, demonstrating that high-resolution  $T_1$ -

weighted images with virtually no bias field can be obtained. As the number of excitations in the GRE block was increased in order to increase the resolution, the flip angle was reduced to maintain the optimum contrast and prevent propagation of the transmission inhomogeneity onto the final image.

## Discussions and conclusions

In this work, we successfully implemented a MP2RAGE sequence, showed a new way to combine these images that has improved noise propagation characteristics and optimized its contrast for brain tissues at 3 and 7 T. The contrast obtained was independent of  $B_1^-$ ,  $T_2^*$  and proton density. Furthermore, optimization of the flip angles allowed creating MP2RAGE images that were largely independent from the transmission  $B_1$  field,  $B_1^+$ . Therefore, this methodology is of great utility in the context of large  $B_1$  field inhomogeneities as those found at high fields ( $\geq 3$  T). Given the long TR and low flip angles used, the sequence is very low SAR intensive making a further attractive option for high field imaging where SAR is often a limitation.

As opposed to other bias field cancellation methodologies, in the MP2RAGE approach, there is no need to perform a co-registration between the two images that have significantly different contrasts, thanks to the interleaved nature of the sequence that ensures that the images are inherently co-registered. In conventional MPRAGE imaging, to ensure that the CSF signal has the same sign as WM and GM, the inversion time is often chosen to be longer than the optimum value, which is not optimal for the contrast between the different tissues. On the other hand, the contrast of the MP2RAGE image was optimized for the differences in  $T_1$  between CSF, GM, and WM observed and, as two images are acquired, it was possible to retrieve the sign of the magnetization and use the whole dynamic range towards tissue contrast. Taking into account the  $T_1$  values measured

**Table 2**

$T_1$  values (mean and standard deviation of the mean) obtained for various different brain tissues at 3 and 7 T.

	Mean ROI volume (mm <sup>3</sup> )	$T_1$ (s)	
		3 T	7 T
White matter	1029	0.81 ± 0.03	1.15 ± 0.06
Corpus callosum	491	0.78 ± 0.04	1.11 ± 0.06
Nucleus caudate	299	1.25 ± 0.07	1.63 ± 0.09
Putamen	556	1.13 ± 0.07	1.52 ± 0.09
Pallidum	191	0.97 ± 0.07	1.17 ± 0.07
Thalamus	306	1.08 ± 0.07	1.43 ± 0.10
Grey matter temporal cortex	524	1.39 ± 0.07	1.97 ± 0.15
Grey matter motor cortex	390	1.32 ± 0.07	1.87 ± 0.17

**Table 3**  
Comparison of  $T_1$  values measured here with those found in the literature.

Study	Field	$T_1$ (s)				Method
		White matter	Putamen	Nucleus caudate	Grey matter	
Wansapura et al. (1999)	3 T	0.79 ± 0.01			1.28 ± 0.02	Saturation recovery, seven TRs, single slice, 3 mm
Lu et al. (2005)	3 T	0.76 ± 0.05	1.10 ± 0.04	1.25 ± 0.06	1.16 ± 0.11	Inversion recovery, 10 TIs, single slice, 6 mm
Wright et al., (2008)	3 T	0.84 ± 0.05	1.33 ± 0.07	1.39 ± 0.05	1.61 ± 0.10	MPRAGE, 8 TIs, 20 slices, 15 mm
This study	3 T	0.81 ± 0.03	1.13 ± 0.07	1.25 ± 0.07	1.35 ± 0.05	MP2RAGE, 160 slice, 1 mm
Rooney et al. (2007)	7 T	1.22 ± 0.03	1.70 ± 0.07	1.75 ± 0.06	2.13 ± 0.10	Look locker sequence, 32 inversion times, single slice, 5 mm
Wright et al., (2008)	7 T	1.13 ± 0.10	1.64 ± 0.16	1.68 ± 0.07	1.93 ± 0.15	MPRAGE, 8 TIs, 20 slices, 15 mm
This study	7 T	1.15 ± 0.06	1.52 ± 0.09	1.63 ± 0.09	1.92 ± 0.16	MP2RAGE, 160 slices, 0.9 mm

for GM and WM at 3 and 7 T (see Table 1), the CNR per unit of time (see Eq. 2) between GM and WM was found to increase by 19% from 3 to 7 T for optimum MP2RAGE parameters at each field. This increase is independent from the SNR improvement expected from high fields, demonstrating that moving from 3 to 7 T also offers improved  $T_1$  contrast.

The resulting  $T_1$  values calculated were highly reproducible both across subjects and within the same subject using different scanning parameters (see Fig. 8). MP2RAGE image intensity depends on  $T_1$  in a monotonous way (see Fig. 3) in a range of interest. The exact range in which the  $T_1$ s are expected to be accurate can be estimated from the plot of  $T_1$  as a function of the MP2RAGE signal intensity (Fig. 3) and covers regions where the derivative of that function does not tend to infinity. As can be seen from Fig. 3b, the signal obtained at 3 T was sensitive to  $T_1$ s longer than 500 ms or shorter than 3000 ms, which covers the full extent of  $T_1$  tissue values reported for human brain at 3 T (for which the contrast was optimized). From Figs. 7b and 8c, it appears that the  $T_1$  of CSF is higher than initially assumed for the optimization ( $T_{1CSF} = 2.5$  s). For values that are out of the range derived from the plots, for example, substantially shorter  $T_1$ s such as those found after injection of high concentrations of gadolinium, the calculated  $T_1$  value is not expected to be precise for the present choice of acquisition parameters. With new acquisition parameters (MP2RAGE-TR,  $TI_1$  and  $TI_2$ ), shorter or longer  $T_1$ s could be accurately estimated. Although most  $B_1^+$  dependence of the final image was minimized by RF pulse amplitude optimization, some  $B_1^+$  bias remained as can be seen from Figs. 3c and d. As an example, at 7T, a variation of  $B_1^+$  of 40% implies and error on the  $T_1$  estimation of grey matter of 4.9%. Such small residual dependence of the calculated  $T_1$  on  $B_1^+$  could be further minimized either by using a low resolution  $B_1^+$  map acquired separately combined with a set of lookup tables to account for the varying  $B_1^+$  (Preibisch and Deichmann, 2009), or by introducing a third readout at a third inversion time from which a  $B_1^+$  and a  $T_1$  map would be calculated (Fleisher et al., 2008). While the first approach

would undermine the possibility of straightforwardly performing the online calculation, the second approach would have a penalty on the acquisition time and SNR. Given the results shown in this article, we believe that the careful adjustment of the RF amplitudes is a sufficient approach to mitigate the range of inhomogeneities found up to 7 T. The phantom data acquired at 7 T with an intra-slice  $B_1$  distribution comparable to in vivo data support this assumption.

Most  $T_1$  studies found in literature are very accurate within study, but not necessarily consistent across studies. This can be due to the choice of sequence or its parameters, the fitting routines or not taking into account the efficiency of the inversion and hence, each different study has a well-defined bias or simply very different populations between studies (both age and gender are known to affect longitudinal relaxation times). The  $T_1$  estimates presented here are in a good agreement with previous reports at 3 T (Lu et al., 2005; Wansapura et al., 1999; Wright et al., 2008).  $T_1$  values at 7 T were in agreement, within the experimental error, with previous studies, although both cortical and subcortical grey matter approximately 10% shorter than the study by (Rooney et al., 2007). It should be noted that Rooney et al. studies showed a tendency to overestimate long  $T_1$  tissues such as cortical and subcortical grey matter at lower fields (1.5 T).

The good agreement between the  $T_1$  maps found in the inter-subject (Figs. 7b and c) and intra-subject studies (Figs. 8c and d), and the ability to perform whole-brain scans in clinically acceptable times suggests that this technique could have a huge potential in taking  $T_1$  quantification in the clinical environment. For example, increases in white matter  $T_1$  in tumor regions are a sensitive indicator of patient status or tumor aggressiveness (Steen et al., 1994). The MP2RAGE technique could therefore be of great interest to study, characterize, and quantify tissue changes in various pathologies known to affect  $T_1$  contrast or to quantify contrast changes due to the injection of contrast agents. Its clinical applicability as a  $T_1$ -mapping technique is further enhanced by the possibility, as in our current implementation, to calculate the MP2RAGE image and  $T_1$  maps online without the need of any extra post-processing.

Taking advantage of the reduced number of inversion times, it was possible to perform, to the best of our knowledge unprecedented whole-brain high-resolution  $T_1$  maps ( $0.65 \times 0.65 \times 0.65$  mm<sup>3</sup>) in 12 min (see Fig. 9). At higher fields, the longer  $T_1$  allowed to increase the number of excitations per GRE block without increasing significantly the PSF. Conversely, at 3 T the possibility of using shorter MP2RAGE TRs allowed to obtain 1 mm isotropic whole-brain  $T_1$  maps in 4min 20 s (see Table 1, Subject 5 parameter set 4 from Fig. 7c).

As can be seen in Figs. 5 and 9, arteries appear bright in the MP2RAGE contrast at 7 T and consequently the  $T_1$  maps suggest very low  $T_1$  values. In our 7 T setup where the nonselective inversion pulse is transmitted through a head only RF coil, the arterial signal intensity at the two inversion times is simply that expected from two GRE images that are only distinguishable through the small difference in flip angles as most blood in brain arteries was outside the regions invertible by the head coil. This property has been used by Van de Moortele et al. (2009) to create angiograms. The fact that arterial blood

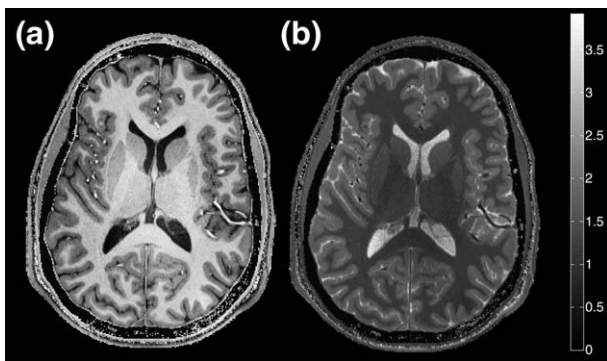


**Fig. 9.** Isotropic 0.65-mm resolution MP2RAGE (a) and  $T_1$  (b) transverse slice taken from a 3D dataset obtained at 7 T with the following parameters: MP2RAGE<sub>TR</sub>/ $TI_1$ / $TI_2$  = 8.0/1.0/3.2 s  $\alpha_1/\alpha_2 = 4^\circ/4^\circ$ . The number of excitations per GRE block was 256, the BW was 200Hz/px, and total acquisition time was 12 min.

has a particular contrast in these images also implies the potential to further improve the outcome of segmentation and classification algorithms that often struggle with distinguishing white matter from arteries (Fischl et al., 2004) and special algorithms have to be developed to remove this information (Penumetcha et al., 2008).

The accuracy of the  $T_1$  is highly dependent on the inversion efficiency of the initial inversion pulse; it is important that the adiabatic condition throughout the entire imaging region is met. At 7 T, due to the increased  $B_1$  field inhomogeneities and usage of a short head only transmit coil, often one side of the bottom of the cerebellum did not meet the adiabatic condition as can be seen in Fig. 5. Such effect is clearly visible as a decrease of the measured  $T_1$  values. This could be improved by, for example, using more efficient adiabatic pulses (Tannus and Garwood, 1997).

Another factor that could influence the estimated  $T_1$  contrast is the point spread function (PSF) along the phase encoding direction looped in the GRE kernel (Deichmann et al., 2000). The  $T_1$  histogram of subject 5 (See Fig. 8c) with an increased flip angle for the first contrast (see parameter set 1 on Table 1) shows lower agreement with respect to the remaining set of parameters. This could be explained, not only to the increased sensitivity to  $B_1$  inhomogeneities of that parameter set, but also to a bigger PSF weighting due to the increased amplitude of the RF pulse of the first gradient echo block. Such PSF problems could be tackled by changing the ordering of the phase encoding steps in order to make the contrast more specific to the centre of k-space (Lin and Bernstein, 2008), which in the referred implementation also allows the reduction of the time needed to acquire whole k-space.

Further developments, such as acquiring the signal at various echo times and with higher acquisition bandwidths to reduce distortions (van der Kouwe et al., 2008), can be combined with the present approach. Initial attempts to perform segmentation by means of conventional segmentation toolboxes such as freesurfer (Dale et al., 1999) have shown very satisfactory results using MP2RAGE images with only one minor alteration to the processing pipeline. Most software packages do not expect images that could have both positive and negative values and hence the MP2RAGE was shifted and scaled to have a range from 0 to 4096 and the regions outside the brain were masked using a manually set threshold on the original contrasts. Segmentation procedures often have difficulties differentiating dura mater from grey matter in MPRAGE images (van der Kouwe et al., 2008). In contrast, the MP2RAGE image, by eliminating the  $M_0$  and  $T_2^*$  contrast, gives a good contrast between GM and dura. These observations, together with the enhanced observation of arteries tissue contrast and the GM, WM, and CSF separation shown in the various whole-brain histograms throughout this study, make the MP2RAGE image suitable for applications requiring segmentation. Furthermore, the inter-subject reproducibility of the signal intensity values and  $T_1$  values obtained suggests that this technique could find applicability in longitudinal studies, group comparison studies, or voxel-based morphometry.

## Acknowledgments

This work was supported by Centre d'Imagerie BioMédicale (CIBM) of the UNIL, UNIGE, HUG, CHUV, EPFL, and the Leenaards and Jeantet Foundations.

## Appendix 1. Derivation of the MP2RAGE signal expression

The MP2RAGE sequence is characterized simply by three types of periods that affect the longitudinal magnetization in the following way:

- a) Longitudinal magnetization is inverted by means of an adiabatic pulse of a given efficiency,  $\text{eff}$ , meaning that  $M_{z,\text{inv}}(M_z(0), \text{eff}) = -\text{eff} M_z(0)$ ;

- b) During the GRE blocks of  $n$  RF pulses with constant flip angles  $\alpha$ , separated by an interval  $TR$ , the longitudinal magnetization evolves in the following way (Deichmann and Haase, 1992):

$$M_{z,\text{nrif}}(M_z(0), T_1, n, TR, \alpha) = M_z(0) \left( \cos(\alpha) e^{-TR/T_1} \right)^n + M_0 \left( 1 - e^{-TR/T_1} \right) \frac{1 - \left( \cos(\alpha) e^{-TR/T_1} \right)^n}{1 - \cos(\alpha) e^{-TR/T_1}}. \quad (\text{A1.1})$$

where  $M_z(0)$  is the longitudinal magnetization at the start of the RF free periods.

- c) During the periods with no RF pulses, the longitudinal magnetization relaxes freely towards equilibrium following the conventional  $T_1$  relaxation expression

$$M_{z,\text{orf}}(M_z(0), T_1, t) = M_z(0) e^{-t/T_1} + M_0 \left( 1 - e^{-t/T_1} \right) \quad (\text{A1.2})$$

A full account of the signal resulting from the MP2RAGE sequence has to take into account the steady-state condition. This implies that the longitudinal magnetization before successive inversions,  $m_{z,ss}$ , has to be the same. Between two successive inversions the  $m_{z,ss}$  undergoes first an inversion (a), followed by recovery for a period  $TA$  (c), a first GRE block (b), a free recovery for a period  $TB$  (c), a second GRE block (b), and a final recovery for a period  $TC$  (c) by the end of which it should be back to its initial value. Mathematically, it is equivalent to solve the following composite equation:

$$m_{z,ss} = M_{z,\text{orf}} \left( M_{z,\text{nrif}} \left( M_{z,\text{orf}} \left( M_{z,\text{nrif}} \left( M_{z,\text{orf}} \left( -\text{eff} \cdot m_{z,ss}, T_1, TA \right), T_1, n, TR, \alpha_1 \right), T_1, TB \right), T_1, n, TR, \alpha_2 \right), T_1, TC \right) \quad (\text{A1.3})$$

where  $TA$ ,  $TB$ , and  $TC$  are the delays described in Fig. 1. Solving this equation for  $m_{z,ss}$  results in the following steady state:

$$m_{z,ss} = \frac{M_0 \left[ \left( \left( (1 - EA) \cos(\alpha_1) E1 \right)^n + (1 - E1) \frac{1 - \cos(\alpha_1) E1}{1 - \cos(\alpha_1) E1} \right)^n EB + (1 - EB) \left( \cos(\alpha_2) E1 \right)^n + (1 - E1) \frac{1 - \cos(\alpha_2) E1}{1 - \cos(\alpha_2) E1} \right] EC + (1 - EC)}{1 + \text{eff} \cos(\alpha_1) \cos(\alpha_2)^n e^{-MP2RAGETR/T_1}} \quad (\text{A1.4})$$

where  $E1 = \exp(-TR/T_1)$ ,  $EA = \exp(-TA/T_1)$ ,  $EB = \exp(-TB/T_1)$ , and  $EC = \exp(-TC/T_1)$ .

Once the steady-state condition is known, the signal for each of the images can be expressed as:

$$\begin{aligned} GRE_{T1} &= B_1^- e^{-TE/T_2^*} M_0 \sin(\alpha_1) \\ &\times \left[ \left( \frac{-\text{eff} \cdot m_{z,ss}}{M_0} EA + (1 - EA) \right) \left( \cos(\alpha_1) E1 \right)^{n/2-1} \right. \\ &\left. + (1 - E1) \frac{1 - \cos(\alpha_1) E1}{1 - \cos(\alpha_1) E1} \right] \end{aligned}$$

$$\begin{aligned} GRE_{T2} &= B_1^- e^{-TE/T_2^*} M_0 \sin(\alpha_2) \\ &\times \left[ \frac{m_{z,ss}}{M_0} - (1 - EC) \right. \\ &\left. - (1 - E1) \frac{\cos(\alpha_2) E1}{1 - \cos(\alpha_2) E1} \right] \quad (\text{A1.5}) \end{aligned}$$

From Eqs. (A4) and (A5), it is clear that when combining the two different images to generate the MP2RAGE image as in Eq. (1), the

dependence in  $B_1^-$ ,  $M_0$ , and  $T_2^*$  will disappear. Assuming a low flip angle regime (where  $\sin(\alpha B_1^+) \sim \alpha B_1^+$  and  $\cos(\alpha B_1^+) \sim 1 + (\alpha B_1^+)^2$ ), the first-order terms, proportional to  $B_1^+$ , of the  $B_1^+$  dependence of the MP2RAGE images is removed, but the  $B_1^+$  terms inside the brackets (implicit in the flip angles) of Eq. (A1.5) will remain (as is demonstrated in Fig. 3).

**Appendix 2. Evaluation of the MP2RAGE combination expression**

In this section, the noise propagation properties of different image combinations will be evaluated. For simplicity, the MP2RAGE image combination (Eq. 1) and the normal image ratio will be defined as functions of  $x$  and  $y$  so that,

$$MP2RAGE = \frac{xy}{x^2 + y^2} \tag{A2.1}$$

$$Ratio = \frac{x}{y}$$

The propagation of noise from  $x$  and  $y$  (which we will assume to be of the same magnitude,  $a$ ) into the final combined image is given by:

$$\sigma_{MP2RAGE} = a \sqrt{\frac{(x^2 - y^2)^2}{(x^2 + y^2)^3}} \tag{A2.2}$$

$$\sigma_{Ratio} = a \sqrt{\frac{x^2 + y^2}{y^4}}$$

The expression obtained for the noise of the MP2RAGE expression suggests that no noise in  $x$  or  $y$  can propagate into the MP2RAGE image if  $x=y$ , this is simply a consequence of both derivatives in  $x$  and  $y$  being zero in those regions.

The SNR of each of the combined images will be given by the ratio of their value and noise propagation characteristics:

$$SNR_{MP2RAGE} = \frac{MP2RAGE}{\sigma_{MP2RAGE}} \Rightarrow \frac{SNR_{MP2RAGE}}{SNR_{Ratio}} = \left| \frac{x^2 + y^2}{x^2 - y^2} \right| \tag{A2.3}$$

$$SNR_{Ratio} = \frac{Ratio}{\sigma_{Ratio}}$$

which implies that when  $x$  or  $y$  is equal to zero, the SNR of the resulting image will be the same, otherwise the SNR of the MP2RAGE combination will be superior to the conventional ratio approach. This conclusion should be valid for any combination of two images with the same noise levels.

**References**

Ashburner, J., Friston, K.J., 2000. Voxel-based morphometry—the methods. *NeuroImage* 11, 805–821.  
 Ashburner, J., Friston, K.J., 2005. Unified segmentation. *NeuroImage* 26, 839–851.  
 Axel, L., Costantini, J., Listerud, J., 1987. Intensity correction in surface-coil MR imaging. *AJR Am. J. Roentgenol.* 148, 418–420.  
 Belaroussi, B., Milles, J., Carme, S., Zhu, Y.M., Benoit-Cattin, H., 2006. Intensity non-uniformity correction in MRI: existing methods and their validation. *Med. Image Anal.* 10, 234–246.  
 Christensen, K.A., Grant, D.M., Schulman, E.M., Walling, C., 1974. Optimal determination of relaxation-times of Fourier-transform nuclear magnetic-resonance—determination of spin-lattice relaxation-times in chemically polarized species. *J. Phys. Chem.* 78, 1971–1977.  
 Cohen, M.S., DuBois, R.M., Zeineh, M.M., 2000. Rapid and effective correction of RF inhomogeneity for high field magnetic resonance imaging. *Hum. Brain Mapp.* 10, 204–211.  
 Dale, A.M., Fischl, B., Sereno, M.I., 1999. Cortical surface-based analysis. I: segmentation and surface reconstruction. *NeuroImage* 9, 179–194.

Deichmann, R., Haase, A., 1992. Quantification of T1 values by Snapshot-Flash NMR imaging. *J. Magn. Reson.* 96, 608–612.  
 Deichmann, R., Hahn, D., Haase, A., 1999. Fast T1 mapping on a whole-body scanner. *Magn. Reson. Med.* 42, 206–209.  
 Deichmann, R., Good, C.D., Josephs, O., Ashburner, J., Turner, R., 2000. Optimization of 3-D MP-RAGE sequences for structural brain imaging. *NeuroImage* 12, 112–127.  
 Deoni, S.C., 2007. High-resolution T1 mapping of the brain at 3T with driven equilibrium single pulse observation of T1 with high-speed incorporation of RF field inhomogeneities (DESPOT1-HIFI). *J. Magn. Reson. Imaging* 26, 1106–1111.  
 Deoni, S.C., Peters, T.M., Rutt, B.K., 2005. High-resolution T1 and T2 mapping of the brain in a clinically acceptable time with DESPOT1 and DESPOT2. *Magn. Reson. Med.* 53, 237–241.  
 Fischl, B., Salat, D.H., van der Kouwe, A.J., Makris, N., Segonne, F., Quinn, B.T., Dale, A.M., 2004. Sequence-independent segmentation of magnetic resonance images. *NeuroImage* 23 (Suppl. 1), S69–S84.  
 Fleysher, R., Fleysher, L., Liu, S., Gonen, O., 2008. TriTone: a radiofrequency field (B1)-insensitive T1 estimator for MRI at high magnetic fields. *Magn. Reson. Imaging* 26, 781–789.  
 Gowland, P., Mansfield, P., 1993. Accurate measurement of T1 in vivo in less than 3 seconds using echo-planar imaging. *Magn. Reson. Med.* 30, 351–354.  
 Katscher, U., Bornert, P., 2006. Parallel RF transmission in MRI. *NMR Biomed.* 19, 393–400.  
 Lin, C., Bernstein, M.A., 2008. 3D magnetization prepared elliptical centric fast gradient echo imaging. *Magn. Reson. Med.* 59, 434–439.  
 Look, D.C., Locker, D.R., 1970. Time saving in measurement of NMR and EPR relaxation times. *Rev. Sci. Instrum.* 41, 250–251.  
 Lu, H., Nagae-Poetscher, L.M., Golay, X., Lin, D., Pomper, M., van Zijl, P.C., 2005. Routine clinical brain MRI sequences for use at 3.0 Tesla. *J. Magn. Reson. Imaging* 22, 13–22.  
 Marques, J.P., Kober, T., van der Zwaag, W., Krueger, G., Gruetter, R., 2008. MP2RAGE, a self-bias field corrected sequence for improved segmentation at high field. *Int. Soc. Magn. Res. Med. Scientific Meeting, Toronto, Canada*, p. 1393.  
 Mugler, J.P., Brookeman, J.R., 1990. Three-dimensional magnetization-prepared rapid gradient-echo imaging (3D MP RAGE). *Magn. Reson. Med.* 15, 152–157.  
 Penumetcha, N., Jedynak, B., Hosakere, M., Ceyhan, E., Botteron, K.N., Ratnanather, J.T., 2008. Segmentation of arteries in MPRAGE images of the ventral medial prefrontal cortex. *Comput. Med. Imaging Graph* 32, 36–43.  
 Preibisch, C., Deichmann, R., 2009. Influence of RF spoiling on the stability and accuracy of T1 mapping based on spoiled FLASH with varying flip angles. *Magn. Reson. Med.* 61, 125–135.  
 Roemer, P.B., Edelstein, W.A., Hayes, C.E., Souza, S.P., Mueller, O.M., 1990. The NMR phased array. *Magn. Reson. Med.* 16, 192–225.  
 Rooney, W.D., Johnson, G., Li, X., Cohen, E.R., Kim, S.G., Ugurbil, K., Springer Jr, C.S., 2007. Magnetic field and tissue dependencies of human brain longitudinal 1H2O relaxation in vivo. *Magn. Reson. Med.* 57, 308–318.  
 Smith, S.M., 2002. Fast robust automated brain extraction. *Hum. Brain Mapp.* 17, 143–155.  
 Steen, R.G., Gronemeyer, S.A., Kingsley, P.B., Reddick, W.E., Langston, J.S., Taylor, J.S., 1994. Precise and accurate measurement of proton T1 in human brain in vivo: validation and preliminary clinical application. *J. Magn. Reson. Imaging* 4, 681–691.  
 Stollberger, R., Wach, P., 1996. Imaging of the active B1 field in vivo. *Magn. Reson. Med.* 35, 246–251.  
 Styner, M., Brechbuhler, C., Szekely, G., Gerig, G., 2000. Parametric estimate of intensity inhomogeneities applied to MRI. *IEEE Trans. Med. Imaging* 19, 153–165.  
 Tannus, A., Garwood, M., 1997. Adiabatic pulses. *NMR Biomed.* 10, 423–434.  
 Thomas, D.L., De Vita, E., Deichmann, R., Turner, R., Ordidge, R.J., 2005. 3D MDEFT imaging of the human brain at 4.7 T with reduced sensitivity to radiofrequency inhomogeneity. *Magn. Reson. Med.* 53, 1452–1458.  
 Van de Moortele, P.-F., Auerbach, E.J., Olman, C., Yacoub, E., Ugurbil, K., Moeller, S., 2008. Unbiased High Resolution T1 Weighted Brain Images at High Field with a New Interleaved 3D-MPRAGE/Proton Density GE sequence. *Annual Meeting Human Brain Mapping Organization, Sidnei*.  
 Van de Moortele, P.F., Auerbach, E.J., Olman, C., Yacoub, E., Ugurbil, K., Moeller, S., 2009. T(1) weighted brain images at 7 Tesla unbiased for Proton Density, T(2)() contrast and RF coil receive B(1) sensitivity with simultaneous vessel visualization. *NeuroImage* 46, 432–446.  
 van der Kouwe, A.J., Benner, T., Salat, D.H., Fischl, B., 2008. Brain morphometry with multiecho MPRAGE. *NeuroImage* 40, 559–569.  
 Vaughan, J.T., Garwood, M., Collins, C.M., Liu, W., DelaBarre, L., Adriany, G., Andersen, P., Merkle, H., Goebel, R., Smith, M.B., Ugurbil, K., 2001. 7T vs. 4T: RF power, homogeneity, and signal-to-noise comparison in head images. *Magn. Reson. Med.* 46, 24–30.  
 Wald, L.L., Carvajal, L., Moyer, S.E., Nelson, S.J., Grant, P.E., Barkovich, A.J., Vigneron, D.B., 1995. Phased array detectors and an automated intensity-correction algorithm for high-resolution MR imaging of the human brain. *Magn. Reson. Med.* 34, 433–439.  
 Wang, J., Qiu, M., Yang, Q.X., Smith, M.B., Constable, R.T., 2005. Measurement and correction of transmitter and receiver induced nonuniformities in vivo. *Magn. Reson. Med.* 53, 408–417.  
 Wansapura, J.P., Holland, S.K., Dunn, R.S., Ball Jr., W.S., 1999. NMR relaxation times in the human brain at 3.0 Tesla. *J. Magn. Reson. Imaging* 9, 531–538.  
 Wright, P.J., Mouglin, O.E., Totman, J.J., Peters, A.M., Brookes, M.J., Coxon, R., Morris, P.E., Clemence, M., Francis, S.T., Bowtell, R.W., Gowland, P.A., 2008. Water proton T1 measurements in brain tissue at 7, 3, and 1.5 T using IR-EPI, IR-TSE, and MPRAGE: results and optimization. *Magma* 21, 121–130.